Journal of Catalysis **209,** 456–471 (2002)
doi:10.1006/jcat.2002.3645

An Investigation of the $NO/H_2/O_2$ (Lean De-NO_x) Reaction on a Highly Active and Selective $Pt/La_{0.7}Sr_{0.2}Ce_{0.1}FeO_3$ Catalyst at Low Temperatures

C. N. Costa,* P. G. Savva,* C. Andronikou,* P. S. Lambrou,* K. Polychronopoulou,* V. C. Belessi,† V. N. Stathopoulos,† P. J. Pomonis,† and A. M. Efstathiou*,[1]

*Department of Chemistry, University of Cyprus, P.O. Box 20537, CY 1678 Nicosia, Cyprus; and †Department of Chemistry, University of Ioannina, Ioannina 45 110, Greece

Received January 7, 2002; revised April 17, 2002; accepted April 23, 2002

A 0.1 wt% Pt supported on $La_{0.7}Sr_{0.2}Ce_{0.1}FeO_3$ solid (mixed oxide containing $LaFeO_3$, $SrFeO_{3-x}$, CeO_2, and Fe_2O_3 phases) has been studied for the $NO/H_2/O_2$ reaction in the 100–400°C range. For a critical comparison, 0.1 wt% Pt was supported on SiO_2, CeO_2, and Fe_2O_3 and tested under the same reaction conditions. For the $Pt/La_{0.7}Sr_{0.2}Ce_{0.1}FeO_3$ catalyst a maximum in the NO conversion (83%) has been observed at 150°C with a N_2 selectivity value of 93%, while for the Pt/SiO_2 catalyst at 120°C (82% conversion) with a N_2 selectivity value of 65% using a GHSV of 80,000 h^{-1}. Low N_2 selectivity values, less than 45%, were obtained with the Pt/CeO_2 and Pt/Fe_2O_3 catalysts in the 100–400°C range. For the $Pt/La_{0.7}Sr_{0.2}Ce_{0.1}FeO_3$ catalyst, addition of 5% H_2O in the feed stream at 140°C resulted in a widening of the operating temperature window with appreciable NO conversion and no negative effect on the stability of the catalyst during 20 h on stream. In addition, a remarkable N_2 yield (93%) after 20 h on 0.25% NO/1% H_2/5% O_2/5% H_2O/He gas stream at 140°C has been observed. Remarkable N_2 selectivity values in the range of 80–90% have also been observed in the 100–200°C low-temperature range either in the absence or in the presence of water in the feed stream. A maximum specific integral reaction rate of 443.5 μmol $N_2/s \cdot g$ of Pt metal was measured at 160°C during reaction with a 0.25% NO/1% H_2/5% O_2/5% H_2O/He gas mixture. This value is higher by 90% than the corresponding one observed on the 0.1 wt% Pt/SiO_2 catalyst at 120°C and it is the highest value ever reported for the reaction at hand in the 100–200°C low-temperature range on Pt-based catalysts. A TOF value of 13.4×10^{-2} s^{-1} for N_2 formation was calculated at 110°C for the $Pt/La_{0.7}Sr_{0.2}Ce_{0.1}FeO_3$ catalyst. Temperature-programmed desorption (TPD) of NO and transient titration experiments of the catalyst surface following $NO/H_2/O_2$ reaction have revealed important information concerning the amount and chemical composition of active and inactive (spectator) adsorbed N-containing species present under reaction conditions.

Key Words: **lean de-NO_x; NO reduction; NO TPD; perovskites.**

1. INTRODUCTION

The selective catalytic reduction (SCR) of NO by NH_3 and hydrocarbons in the presence of excess oxygen has attracted great attention in the last three decades and many reports appeared in the literature as recently reviewed (1–3). Today's great concern about the increasing emissions of carbon dioxide to the atmosphere and the problems resulting from the use of NH_3 as a reducing agent (4) lead to a demand for appropriate non-carbon-containing reducing molecules for the catalytic removal of NO from combustion exhaust streams. Hydrogen is one of the gases present in the exhaust stream of automobiles and has been reported to be very effective as a reducing agent for the NO/H_2 reaction (5–16). Hydrogen could also be used to reduce NO_x emissions of stationary sources. However, only a few attempts have been reported for the reduction of NO by H_2 in oxygen-rich conditions (17–21). The strong competition between adsorbed NO_x and oxygen species for adsorbed hydrogen under the applied reaction conditions (22, 23) makes the development of suitable catalytic systems a difficult task.

Supported platinum catalysts have been found to be the most active for the $NO/H_2/O_2$ lean de-NO_x reaction at low temperatures ($T < 200$°C) (17–21). Yokota *et al.* (20) have reported catalytic results in the NO reduction with H_2 in the presence of O_2 over the Pt–Mo–Na/SiO_2 catalyst, while Machida *et al.* (21) have studied the same reaction over Pt supported on TiO_2, ZrO_2, SiO_2, Al_2O_3, CeO_2, and mixtures of them. Kinetic results of the $NO/H_2/O_2$ reaction on the Pt–Mo–Co/α-Al_2O_3 catalyst have been reported by Frank *et al.* (17). The latter catalyst formulation was found to produce substantially lower amounts of N_2O (N_2 selectivity at about 75%) as compared to conventional supported Pt catalysts (e.g., Pt/Al_2O_3, SiO_2), which are known to present lower N_2 selectivity values ($S_{N_2} = 40$–60%).

We have already reported various results of the catalytic performance of the $Pt/La_{0.5}Ce_{0.5}MnO_3$ catalyst (24) toward

[1] To whom correspondence should be addressed. Fax: (+35722)-339063. E-mail: efstath@ucy.ac.cy.

0021-9517/02 $35.00

the NO/H_2/O_2 reaction. It was found (24) that this catalyst exhibits remarkable specific activity and N_2 selectivity values ($S_{N_2} = 80$–90%), a wide operating temperature window, and a small positive effect on the N_2 yield when 5% H_2O was added in the feed stream in the 100–200°C range.

In the present work, another mixed oxidic/perovskitic solid material containing La, Sr, Ce, and Fe metals has been investigated as a support of Pt metal toward the NO/H_2/O_2 lean de-NO_x reaction. This catalytic system exhibits a remarkably high stability and N_2 yield (93%) in the presence of 5% H_2O in the NO/H_2/O_2 feed stream at 140°C after 20 h on stream, and the best-ever reported mean conversion of NO in the operating temperature range of 100–200°C. In the case of Pt/$La_{0.5}Ce_{0.5}MnO_3$ catalyst (24), a corresponding N_2 yield value lower by 15 percentage units, a mean conversion value lower by 17 percentage units, and a significantly smaller temperature window (ΔT) of operation in the 100–250°C range as compared to the present Pt/La–Sr–Ce–Fe–O catalyst were reported. These features suggest that the present La–Sr–Ce–Fe–O mixed oxidic/perovskitic support material has significantly improved the performance of supported Pt metal toward the NO/H_2/O_2 lean de-NO_x reaction compared to the La–Ce–Mn–O mixed oxidic/perovskitic support material (24).

The present work concerns catalytic and transient reactivity studies on a 0.1 wt% Pt/$La_{0.7}Sr_{0.2}Ce_{0.1}FeO_3$ catalyst for both the NO/H_2/O_2 and NO/H_2 reactions. Similar studies were also conducted on 0.1 wt% Pt/SiO_2, Pt/CeO_2, and Pt/Fe_2O_3 catalysts for a critical comparison and to gain insight into the role of support phase toward the present reaction. The transient studies involved (a) temperature-programmed desorption (TPD) of NO, (b) temperature-programmed surface reaction (TPSR) in He flow following NO/H_2/O_2 reaction, and (c) TPSR in H_2/He flow following the NO/H_2/O_2 reaction. The latter two kinds of transient experiments allowed for the estimation of the surface coverage of adsorbed active and inactive NO_x species and that of the total N-containing intermediate species formed under NO/H_2/O_2 reaction conditions. The surface reactivity of the various NO_x adsorbed species toward He and H_2/He treatment has also been probed.

2. EXPERIMENTAL

2.1. Catalyst Preparation

The $La_{0.7}Sr_xCe_{0.3-x}FeO_3$ solids were prepared using the ceramic method as previously reported (24) from calculated amounts of $La(NO_3)_3 \cdot 6H_2O$ (Merck), $Sr(NO_3)_2$ (Ferak), $Fe(NO_3)_3 \cdot 9H_2O$ (Merck), and CeO_2 (Aldrich). It is mentioned that the notation $La_{0.7}Sr_xCe_{0.3-x}FeO_3$ indicates just the nominal composition of the solids. This has nothing to do with particular crystal phases existing in each sample.

The 0.1 wt% Pt-supported catalysts (Pt/$La_{0.7}Sr_{0.2}Ce_{0.1}FeO_3$, Pt/$SiO_2$, Pt/$CeO_2$, and Pt/$Fe_2O_3$) were prepared by the wet impregnation method using the $H_2Pt(IV)Cl_6$ (Aldrich) precursor. The SiO_2 support (Aldrich) used was of standard grade (325 mesh), while the CeO_2 (Aldrich) and Fe_2O_3 (Aldrich) were of 99.9 and 99.98% purity, respectively. After impregnation and drying (overnight at ~120°C), the catalyst sample was calcined in air at 400°C for 2 h prior to use.

2.2. Catalyst Characterization

2.2.1. Surface area and metal dispersion measurements. The specific surface area of all support materials was checked by N_2 adsorption at 77 K (BET method) using a multipoint Fisons Sorpty 1900 System. Metal dispersions of the supported metal catalysts were determined by H_2 chemisorption at room temperature followed by TPD in He flow (24).

2.2.2. XRD analysis. The crystal structure of the prepared $La_{0.7}Sr_xCe_{0.3-x}FeO_3$ solids was checked by XRD measurements using a SIEMENS Diffract 500 system employing Cu$K\alpha$ radiation ($\lambda = 1.5418$ Å).

2.2.3. Mössbauer studies. ^{57}Fe Mössbauer spectra were obtained for the prepared $La_{0.7}Sr_xCe_{0.3-x}FeO_3$ solids at 300 and 20 K, using a closed loop refrigerator system. These results have been reported and discussed in a previous work (25).

2.3. Catalytic and Transient Studies

The flow system used for conducting catalytic measurements for the NO/H_2/O_2 reaction at 1 atm total pressure was previously described (24, 26). A feed stream consisting of 0.25% NO, 1.0% H_2, 5% O_2, and He as balance gas was used in all experiments. The latter mixture was prepared from a 0.942% NO/He (Praxair, ±2% relative accuracy), 20% O_2/He (Praxair, ±2% relative accuracy), and pure H_2 (Linde–Hellas, 99.999%) gases. The amount of catalyst sample used in all catalytic experiments was 0.15 g and the total flow rate was 100 cm^3 (STP)/min, resulting in a GHSV of about 80,000 h^{-1}. Details of the experiments to study the effects of H_2O in the feed stream on the NO conversion and N_2 selectivity have been described (24).

According to the GC/MS analyses performed for the present reaction system, H_2 reacts with NO and O_2 on the basis of the following competitive reaction scheme:

$$2NO + 4H_2 + O_2 \rightarrow N_2 + 4H_2O, \quad [1]$$

$$2NO + 3H_2 + O_2 \rightarrow N_2O + 3H_2O, \quad [2]$$

$$H_2 + 1/2O_2 \rightarrow H_2O. \quad [3]$$

Some details of the GC/MS analysis are as follows. The detection of NO_2 in the reaction product and the prepared

TABLE 1

Sensitivity, Background, and Detection Limits of NO, N_2O, NO_2, and N_2 Molecular Species Used in the Mass Spectrometer for the GC/MS Analysis Described in Section 2.3

Gas	Sensitivity (amps/ppm)	Background[a] (amps)	Detection limit[b] (amps)
NO at $m/z=30$	7.44×10^{-15}	5.2×10^{-13}	$2.2\times10^{-14}=3$ ppm
N_2O at $m/z=44$	$0.763\times$ sens(NO)	6.3×10^{-13}	$2.8\times10^{-14}=5$ ppm
NO_2 at $m/z=46$	$0.19\times$ sens(NO)	3.7×10^{-13}	$8.0\times10^{-15}=6$ ppm
N_2 at $m/z=28$	$1.80\times$ sens(NO)	1.08×10^{-12}	$3.1\times10^{-14}=2$ ppm

[a] The background values were obtained under a flow of a 4% O_2/He gas mixture in the mass spectrometer. It was found that about a 5% difference in the background values obtained in He or the 4% O_2/He gas mixture exists. A 4% O_2/He gas mixture was used since it simulates the background conditions for the indicated molecular species in the ion source of the mass spectrometer for the reaction product gas stream. Important ion source conditions used: 70 eV, SEM = 850 V.

[b] A ratio of two for the signal to noise is considered.

feed gas (bypass the reactor) was checked by mass spectrometer (mass number $m/z=46$). There is no contribution to this mass number from any other molecular species that could possibly be present in the reaction system at hand. When the $NO/H_2/O_2$ feed gas mixture was passed bypassing the reactor, no NO_2 signal in the mass spectrometer was observed within the detection limits of the analysis. This result suggests that no gas-phase reaction between the NO and O_2 used to form NO_2 in the heated lines of the flow system and the mass spectrometer occurred. The values of the background, sensitivity, and detection level of NO_2 and those related to the other molecular species measured by the mass spectrometer are given in Table 1. Based on the mass spectrometry analysis of NO_2, the above-mentioned reaction scheme (Eqs. [1]–[3]) is proposed.

The presence of N_2O in the product gas stream was checked and quantified by two independent measurements. The first one was based on the use of gas chromatography (Poropak Q (80/100 mesh) column, TCD detector) and the second one on the use of mass spectrometry, after using the equation

$$I_{44} = y(N_2O) \times \text{sens}(N_2O), \qquad [4]$$

where I_{44} is the mass spectrometer signal (Amps) corresponding to the mass number $m/z=44$ (after background subtraction), $y(N_2O)$ is the mole fraction (ppm) of N_2O gas, and sens (N_2O) is the sensitivity (Amps/ppm) of N_2O gas. Both GC and MS independent measurements of N_2O were found to agree within 3%.

The presence of N_2 in the product gas stream was also checked and quantified by two independent measurements. The first one was based on the use of gas chromatography (Molecular Sieve 5A (80/100 mesh) column, TCD detector) and the second one on the use of mass spectrometry, after using the equation

$$I_{28} = y(N_2) \times \text{sens}(N_2) + y(N_2O) \times \text{sens}(N_2O) \times \text{cc}(28/44), \qquad [5]$$

where I_{28} is the mass spectrometer signal corresponding to the mass number $m/z=28$, $y(N_2)$ is the mole fraction of N_2 gas, sens(N_2) is the sensitivity of N_2 gas, and cc(28/44) is the cracking coefficient for the N_2O molecular species in the mass spectrometer given as the ratio of the signal intensities obtained at $m/z=28$ and 44 for N_2O. Both GC and MS independent measurements of N_2 were found to agree within 3%.

The measurement of NO in the reaction product and feed gas (bypassing the reactor) stream was made by mass spectrometry. The mass numbers $m/z=30$, 44, and 46 (scan mode) were used along with the equation

$$I_{30} = y(NO) \times \text{sens}(NO) + y(N_2O) \times \text{sens}(N_2O) \times \text{cc}(30/44) + y(NO_2) \times \text{sens}(NO_2) \times \text{cc}(30/46), \qquad [6]$$

where I_{30} is the mass spectrometer signal corresponding to the mass number $m/z=30$, $y(NO)$ is the mole fraction of NO gas, sens(NO) is the sensitivity of NO gas, and cc(30/44) and cc(30/46) are the cracking coefficients for the N_2O and NO_2 molecular species in the mass spectrometer, respectively, contributing to the signal at $m/z=30$. Equation [6] provides the means of calculating the mole fraction of NO after measuring the mole fractions of N_2O and NO_2 according to the procedures described above.

The accuracy of the analysis of N_2, N_2O, NO, and NO_2 according to the procedures mentioned in the previous paragraphs has also been checked by the N-atomic material balance (at steady state) given by the equation

$$F_t^{in} \cdot y^f(NO) = F_t^{out} \cdot [y(NO) + 2y(N_2O) + 2y(N_2) + y(NO_2)], \qquad [7]$$

where F_t^{in} and F_t^{out} are the total molar rates (mol/s) of feed and product gas stream at the inlet and outlet of the reactor, respectively, and $y^f(NO)$ is the feed mole fraction of NO. The material balance equation [7] was satisfied within 3–5% in all experiments performed. Gas sensitivities and cracking coefficients were measured based on certified gas mixtures of the molecular species of interest in He diluent gas.

Steady state reaction rates (kinetic or integral) were calculated using the relationship Rate $(\text{mol}\cdot\text{g}^{-1}\cdot\text{s}^{-1}) = F_t^{out} y_i / W$, where y_i is the molar fraction of component i (e.g., N_2) expressed in ppm $\times 10^{-6}$, and W is the weight of the catalyst (g). Reaction turnover frequencies (TOF, s^{-1}) were calculated on the basis of the exposed Pt atoms (μmol of Pt_s/g_{cat}).

The selectivity, α, for the reduction of NO by H_2 to N_2, e.g., the ratio of the consumption rate of H_2 for reaction [1]

TABLE 2

Description of Sequential Step Changes of Gas Flow during Temperature-Programmed Desorption (TPD) and Surface Reaction (TPSR) Experiments

Experiment	Sequence of step changes of gas flow over the catalyst sample
A	0.5% NO/He (room temperature, 20 min) → He (5 min, room temperature) → TPD in He
B	0.25% NO/1.0% H_2/5% O_2 (140°C, 30 min) → cool quickly to room temperature in reaction mixture → He (5 min, 30°C) → TPSR in He
C	0.25% NO/1.0% H_2/5% O_2 (140°C, 30 min) → cool quickly to room temperature in reaction mixture → He (5 min, 30°C) → TPSR in 10% H_2/He

to the total consumption rate of H_2 (reactions [1]–[3]), is calculated on the basis of the equation

$$\alpha(\%) = \frac{0.5 y^{f}_{NO} X_{NO}}{y^{f}_{H_2} X_{H_2}} \times S_{N_2} \times 100. \quad [8]$$

In Eq. [8] y^{f}_{NO} and $y^{f}_{H_2}$ are the feed molar fractions of NO and H_2, respectively, X_{NO} and X_{H_2} are the NO and H_2 conversions, respectively, and S_{N_2} is the selectivity of the reaction to N_2 gas product. The value of 0.5 is the stoichiometric ratio of NO to H_2 appeared in reaction [1].

Temperature-programmed desorption (TPD) and surface reaction (TPSR) experiments were conducted in a specially designed flow system that has been recently described (26). For transient experiments, the amount of catalyst sample used was 0.15–0.2 g. The total flow rate was kept constant at 30 cm^3 (STP)/min. Chemical analysis of the gas effluent stream of reactor during transients was done with an *online* quadrupole mass spectrometer previously described (24, 26). The gaseous responses obtained by mass spectrometry were calibrated against standard mixtures. The mass numbers (m/z) 15, 28, 30, 32, 44, and 46 were used for NH_3, N_2, NO, O_2, N_2O, and NO_2, respectively.

Table 2 describes the necessary sequence of steps performed for each kind of transient experiment presented in this work. The underlined step is that during which measurements by *online* mass spectrometry were recorded.

3. RESULTS

3.1. Catalyst Characterization

3.1.1. BET surface area measurements. The specific surface areas (BET, m^2/g) of the $La_{0.7}Sr_xCe_{0.3-x}FeO_3$ solids were evaluated on the basis of results obtained from the measured nitrogen isotherms at 77 K. The BET areas were found to be in the 3–4 m^2/g range. In the case of SiO_2, CeO_2, and Fe_2O_3 the BET areas were found to be 140, 45, and 7.6 m^2/g, respectively. Before any measurements were taken, the sample was outgassed at 250°C under vacuum ($P \approx 1.3 \times 10^{-3}$ mbar) overnight.

3.1.2. X-ray diffraction studies. The crystal phases present in the $La_{0.7}Sr_xCe_{0.3-x}FeO_3$ solids were determined by XRD with reference to ASTM standards and are shown in Table 3. The main crystal phases detected are the $LaFeO_3$ and $SrFeO_{3-x}$ of perovskite structure and the oxidic phases of CeO_2 and Fe_2O_3.

3.1.3. Metal dispersion. The dispersion of platinum for each of the 0.1 wt% Pt/SiO_2 and 0.1 wt% Pt/$La_{0.7}Sr_{0.2}Ce_{0.1}FeO_3$ catalysts was found to be about 90% (4.5 ± 0.1 μmol Pt_s/g_{cat}) on the basis of H_2 chemisorption followed by TPD (24). In the case of Pt/CeO_2 and Pt/Fe_2O_3 catalysts, dispersion values of 84 and 75%, respectively, were estimated. It is noted that no H_2 spillover effect was found under the H_2 chemisorption conditions applied (24).

3.2. Catalyst Performance and Stability with Time on Stream

3.2.1. $La_{0.7}Sr_xCe_{0.3-x}FeO_3$ solids. Four solids of the $La_{0.7}Sr_xCe_{0.3-x}FeO_3$ series (Table 3) were tested for the NO/H_2/O_2 lean de-NO_x reaction in the 200–500°C range. With a 0.25% NO/1% H_2/5% O_2/He feed gas composition at 30,000 h^{-1} GHSV, the $La_{0.7}Sr_{0.2}Ce_{0.1}FeO_3$ solid had shown the best catalytic performance in terms of NO conversion and N_2 selectivity. NO conversions in the 20–38% range and N_2 selectivity values in the 89–98% range between 350 and 500°C had been observed. The $La_{0.7}Sr_{0.2}Ce_{0.1}FeO_3$ solid was chosen to be used as a support for the preparation of the 0.1 wt% Pt/$La_{0.7}Sr_{0.2}Ce_{0.1}FeO_3$ catalyst on the basis of these results.

3.2.2. Pt/$La_{0.7}Sr_{0.2}Ce_{0.1}FeO_3$ and Pt/SiO_2 catalysts. Figures 1 and 2 present results of the catalytic behavior of the 0.1 wt% Pt/$La_{0.7}Sr_{0.2}Ce_{0.1}FeO_3$ solid as a function of reaction temperature for the NO/H_2/O_2 reaction. The temperature of 400°C was the highest investigated in order to avoid sintering of the Pt metal. In the 100–220°C low-temperature range, the catalyst presents high catalytic activity ($X_{NO} > 20\%$), with a maximum conversion of 83%

TABLE 3

Prepared $La_{0.7}Ce_xSr_{0.3-x}FeO_3$ Solids and Crystal Phases Detected by XRD

Solid composition	Crystal phases
$La_{0.7}Ce_{0.3}FeO_3$	$LaFeO_3/Fe_2O_3/CeO_2/La(OH)_3$[a]
$La_{0.7}Sr_{0.3}FeO_3$	$LaFeO_3/SrFeO_{3-x}/SrFeLaO_4$[a]/$La(OH)_3$[a]/$SrFe_{12}O_{19}$[a]
$La_{0.7}Sr_{0.1}Ce_{0.2}FeO_3$	$LaFeO_3/Fe_2O_3/CeO_2/SrFeO_{3-x}/La(OH)_3$[a]/$SrFe_{12}O_{19}$[a]
$La_{0.7}Sr_{0.2}Ce_{0.1}FeO_3$	$LaFeO_3/SrFeO_{3-x}/Fe_2O_3/CeO_2/La(OH)_3$[a]

[a] Traces.

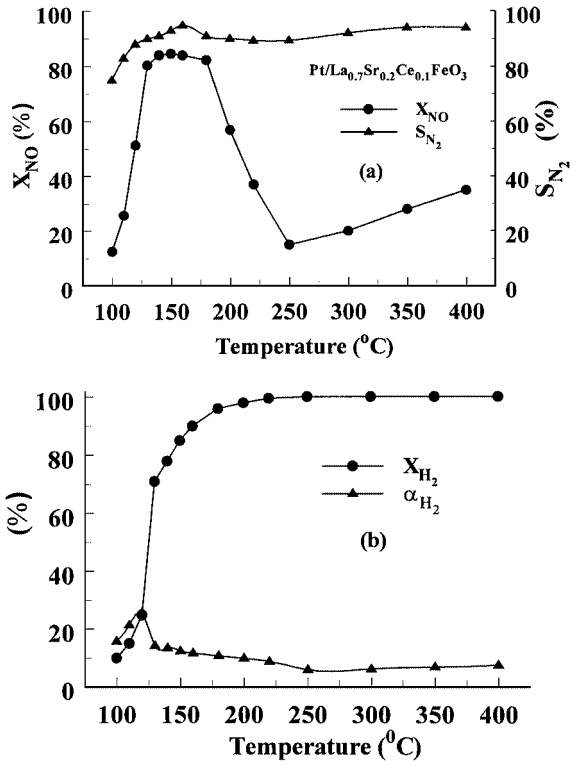

FIG. 1. Temperature profiles of (a) the NO conversion (X_{NO} (●)) and N_2 selectivity (S_{N_2} (▲)) and (b) the H_2 conversion (X_{H_2} (●)) and H_2 reaction selectivity (α_{H_2} (▲)) of the NO/H_2/O_2 lean de-NO_x reaction on the 0.1 wt% Pt/$La_{0.7}Sr_{0.2}Ce_{0.1}FeO_3$ catalyst. Reaction conditions: $H_2 = 1.0\%$, $NO = 0.25\%$, $O_2 = 5\%$, $W = 0.15$ g, GHSV = 80,000 h^{-1}.

at 150°C (Fig. 1a). Between 250 and 300°C the activity of the catalyst is small, while in the 300–400°C high-temperature range the NO conversion is between 20 and 38%. The latter behavior is mostly due to the activity of the support itself.

Based on the results shown in Fig. 1a, the Pt/La–Sr–Ce–Fe–O catalyst is highly selective toward N_2 formation, with selectivity values in the 77–93% range. The N_2 selectivity increases from 77 to 90% in the 100–150°C range, while it practically remains unchanged at temperatures higher than 150°C (S_{N_2} = 90–93%). As shown in Fig. 1b, the H_2 conversion increases significantly with reaction temperature in the 100–200°C range, where a value of about 98% (practically a complete conversion) is obtained at 300°C. This temperature profile of H_2 conversion is totally different than that of the NO conversion seen in Fig. 1a. As the temperature of the reaction increases, the percentage of H_2 used for the desired reaction [1] decreases due to the H_2 combustion reaction [3]. It is shown later that the rate of H_2 combustion is about 15 times higher than the rate of NO/H_2/O_2 reaction, and this explains the temperature profile of the H_2 reaction selectivity parameter, α_{H_2}(%), shown in Fig. 1b.

Figure 2 presents comparative results concerning the integral rates per gram of catalyst of N_2 (Fig. 2a) and N_2O (Fig. 2b) formation for the 0.1 wt% Pt/$La_{0.7}Sr_{0.2}Ce_{0.1}FeO_3$ and 0.1 wt% Pt/SiO_2 catalysts in the 100–400°C range. At temperatures higher than 250°C the 0.1 wt% Pt/$La_{0.7}Sr_{0.2}Ce_{0.1}FeO_3$ catalyst exhibits significant rates of N_2 formation with respect to the 0.1 wt% Pt/SiO_2 catalyst; there is practically no activity of Pt/SiO_2 in the 250–400°C range. For the former catalyst, an increasing reaction rate is observed in the 250–400°C range. At 400°C a rate similar to that obtained at 120°C was estimated. In contrast, the Pt/SiO_2 catalyst presents significantly higher rates of N_2O production compared to Pt/$La_{0.7}Sr_{0.2}Ce_{0.1}FeO_3$ in the 100–150°C range (Fig. 2b). In particular, the rate of N_2O formation on the Pt/SiO_2 is found to be four times higher than that obtained on the Pt/$La_{0.7}Sr_{0.2}Ce_{0.1}FeO_3$ catalyst at 150°C. It is apparent, therefore, that the use of $La_{0.7}Sr_{0.2}Ce_{0.1}FeO_3$ solid instead of SiO_2 as support of Pt metal significantly improved the N_2 selectivity of Pt in the 100–200°C low-temperature range.

It was of interest to study the rate of NO decomposition in the 200–400°C range, in which the H_2 conversion is very high (Fig. 1b). After using a 0.25% NO/He gas mixture over the Pt/$La_{0.7}Sr_{0.2}Ce_{0.1}FeO_3$ catalyst, it was found that the rate of NO decomposition toward N_2 formation

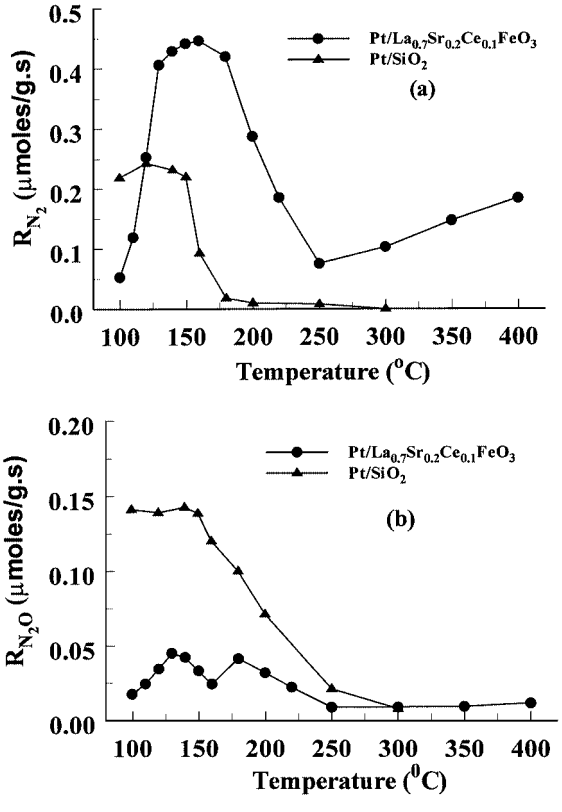

FIG. 2. Temperature profiles of (a) the N_2 and (b) the N_2O integral production rates for the NO/H_2/O_2 lean de-NO_x reaction on the 0.1 wt% Pt/$La_{0.7}Sr_{0.2}Ce_{0.1}FeO_3$ (●) and 0.1 wt% Pt/SiO_2 (▲) catalysts. Reaction conditions: $H_2 = 1.0\%$, $NO = 0.25\%$, $O_2 = 5\%$, $W = 0.15$ g, GHSV = 80,000 h^{-1}.

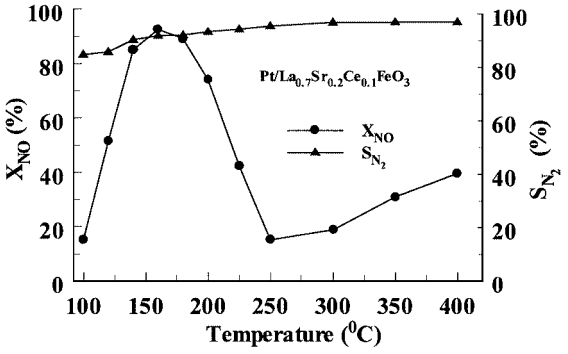

FIG. 3. Effect of 5% H_2O in the feed stream on NO conversion (●) and N_2 selectivity (▲) as a function of reaction temperature on the 0.1 wt% $Pt/La_{0.7}Sr_{0.2}Ce_{0.1}FeO_3$ catalyst. Reaction conditions: NO = 0.25%, H_2 = 1.0%, O_2 = 5%, H_2O=5%, W = 0.15 g, GHSV = 80,000 h^{-1}.

in the 200–350°C range was less than 5% of the rate of N_2 formation from the NO/H_2/O_2 reaction mixture.

The catalytic performance of the $Pt/La_{0.7}Sr_{0.2}Ce_{0.1}FeO_3$ solid was also studied in the presence of 5 mol% H_2O in the feed stream containing 0.25 mol% NO, 1.0 mol% H_2, 5 mol% O_2, and He as balance gas, and results are presented in Fig. 3. Based on the results presented in Figs. 1 and 3, the presence of water in the reaction stream affected significantly the activity of the catalyst in the 100–200°C range but only slightly at $T > 250$°C. The N_2 selectivity is rather slightly affected (less than 5%) by the presence of water in the feed in the 100–400°C range. A N_2 selectivity value of about 95% is obtained in the 300–400°C range.

Integral rates per gram of catalyst of N_2 and N_2O formation for the $Pt/La_{0.7}Sr_{0.2}Ce_{0.1}FeO_3$ and Pt/SiO_2 catalysts in the 100–400°C range in the case where H_2O is present in the feed stream are given in Fig. 4. The $Pt/La_{0.7}Sr_{0.2}Ce_{0.1}FeO_3$ catalyst exhibits significantly higher rates of N_2 formation than the Pt/SiO_2 catalyst above 140°C, where at $T > 250$°C the activity of $Pt/La_{0.7}Sr_{0.2}Ce_{0.1}FeO_3$ increases with reaction temperature. No activity is observed in the case of Pt/SiO_2 catalyst at $T > 220$°C, a result similar to that observed in the absence of water in the feed stream (Fig. 2). The Pt/SiO_2 presents much higher rates of N_2O formation than the $Pt/La_{0.7}Sr_{0.2}Ce_{0.1}FeO_3$ catalyst in the 100–150°C range. It should be pointed out that there is a positive effect of water on Pt/SiO_2 in reducing significantly the rate of N_2O formation in the 100–250°C range (compare Figs. 2b and 4b).

Figure 5 presents results on the stability with time on stream of the catalytic performance in terms of N_2 product yield (Y_{N2},%) of the $Pt/La_{0.7}Sr_{0.2}Ce_{0.1}FeO_3$ and Pt/SiO_2 solids at 140°C. It is observed that for both catalysts the N_2 yield changes only by 10 percentage units during the first 5 h of reaction. In the case of Pt/SiO_2, the N_2 yield decreases with a low rate for the next 15 h on stream, while in the case of $Pt/La_{0.7}Sr_{0.2}Ce_{0.1}FeO_3$ it increases by 30 percentage units. For the latter catalyst, there is an increase in the initial N_2 product yield by about 15 percentage units after 20 h on stream. It is also important to note that the $Pt/La_{0.7}Sr_{0.2}Ce_{0.1}FeO_3$ catalyst exhibits a remarkable N_2 yield value of 93% after 20 h on stream, a value higher by 40 percentage units than that obtained with the Pt/SiO_2 catalyst (Fig. 5).

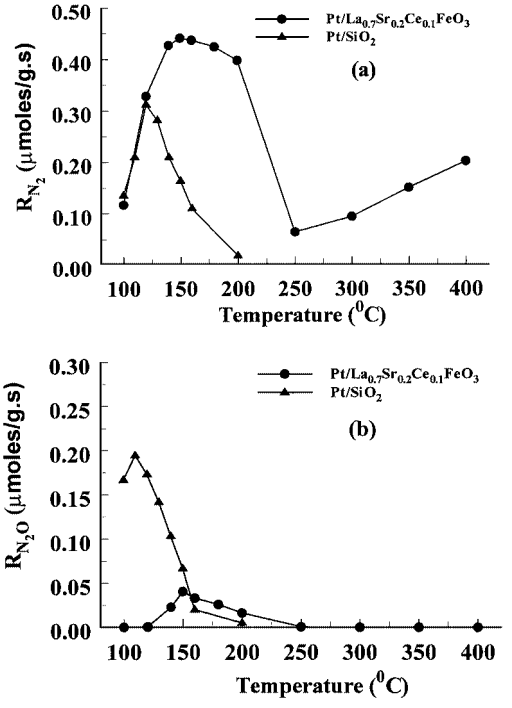

FIG. 4. Effect of 5% H_2O in the feed stream on (a) integral reaction rate of N_2 and (b) N_2O formation on the 0.1 wt% $Pt/La_{0.7}Sr_{0.2}Ce_{0.1}FeO_3$ (●) and 0.1 wt% Pt/SiO_2 (▲) catalysts. Reaction conditions: H_2 = 1.0%, NO = 0.25%, O_2 = 5%, H_2O = 5%, W = 0.15 g, GHSV = 80,000 h^{-1}.

3.2.3. Pt/CeO_2 and Pt/Fe_2O_3 catalysts. In an effort to elucidate the remarkable catalytic performance of the 0.1 wt% Pt/La–Sr–Ce–Fe–O solid composition previously presented, catalytic experiments similar to those presented

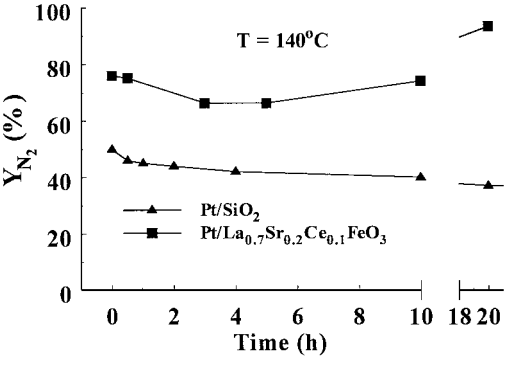

FIG. 5. Stability test on the 0.1 wt% $Pt/La_{0.7}Sr_{0.2}Ce_{0.1}FeO_3$ (■) and 0.1 wt% Pt/SiO_2 (▲) catalysts. Reaction conditions: H_2 = 1.0%, NO = 0.25%, O_2 = 5%, H_2O = 5.0%, T = 140°C, W = 0.15 g, GHSV = 80,000 h^{-1}.

in Fig. 1a were conducted on the 0.1 wt% Pt/CeO_2 and 0.1 wt% Pt/Fe_2O_3 catalysts. The choice of study of the oxidic phases of CeO_2 and Fe_2O_3 as supports of Pt metal was due to the fact that these metal oxide phases were present in the $La_{0.7}Sr_{0.2}Ce_{0.1}FeO_3$ support composition (Table 3). The preparation of pure $LaFeO_3$ and $SrFeO_{3-x}$ crystal phases by the same ceramic method followed here was not possible. In particular, it seems very difficult to prepare a pure $SrFeO_{3-x}$ crystal phase with the same x value as that found in the $La_{0.7}Sr_{0.2}Ce_{0.1}FeO_3$ solid composition. For these reasons, the catalytic performance of supported Pt on each of these two phases is not presented.

Based on the results shown in Fig. 6, the following are noted. Both catalyst formulations exhibit N_2 selectivity values lower than 45% in the 100–250°C low-temperature range of interest, while selectivity values in the 75–90% range are obtained in the case of $Pt/La_{0.7}Sr_{0.2}Ce_{0.1}FeO_3$ solid (Fig. 1a). On the other hand, the Pt/CeO_2 system presents remarkably high activity values for the conversion of NO in the 100–250°C range, similar to the ones obtained with the $Pt/La_{0.7}Sr_{0.2}Ce_{0.1}FeO_3$ solid (compare Figs. 1a and 6a). However, in terms of activity toward N_2 formation, the Pt/CeO_2 system presents a value of 200 μmol/g of Pt · s compared to the value of 390 μmol/g of Pt · s obtained with $Pt/La_{0.7}Sr_{0.2}Ce_{0.1}FeO_3$ at 150°C. In the case of Pt/Fe_2O_3 system, much lower X_{NO} values and specific N_2 reaction rates are obtained (13.0 μmol/g of Pt · s at 150°C).

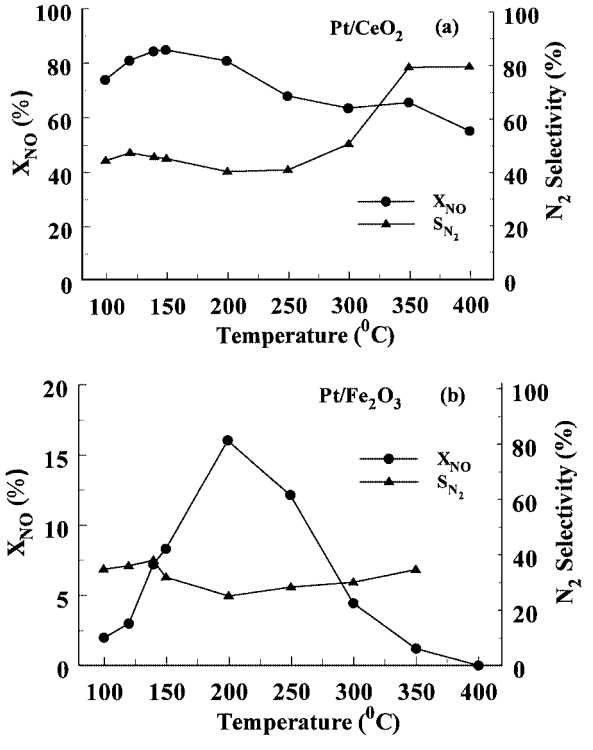

FIG. 6. Temperature profiles of the NO conversion (X_{NO} (●)) and N_2 selectivity (S_{N_2} (▲)) of the $NO/H_2/O_2$ lean de-NO_x reaction on (a) 0.1 wt% Pt/CeO_2 and (b) 0.1 wt% Pt/Fe_2O_3 catalysts. Reaction conditions: $H_2 = 1.0\%$, $NO = 0.25\%$, $O_2 = 5\%$, $W = 0.15$ g, GHSV = 80,000 h^{-1}.

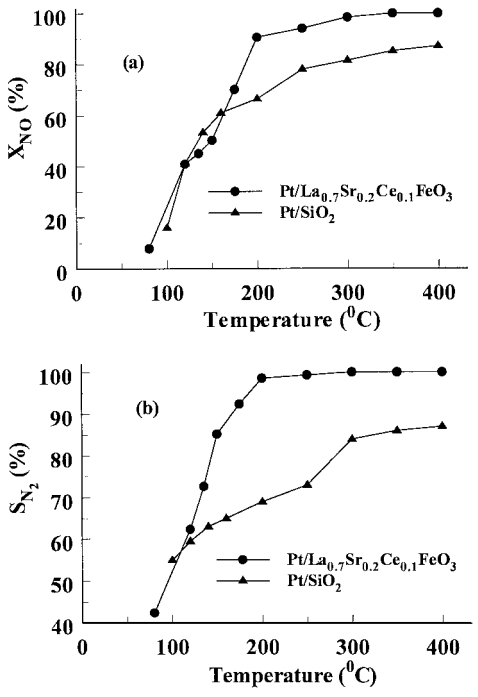

FIG. 7. Temperature profiles of (a) the NO conversion and (b) the N_2 selectivity for the NO/H_2 reaction on the 0.1 wt% $Pt/La_{0.7}Sr_{0.2}Ce_{0.1}FeO_3$ (●) and 0.1 wt% Pt/SiO_2 (▲) catalysts. Reaction conditions: $H_2 = 1.0\%$, $NO = 0.25\%$, $W = 0.15$ g, GHSV = 80,000 h^{-1}.

3.3. Catalyst Performance for the NO/H₂ Reaction

Of interest was the study of the catalytic performance of $Pt/La_{0.7}Sr_{0.2}Ce_{0.1}FeO_3$ and Pt/SiO_2 solids toward the NO/H_2 reaction (in the absence of oxygen in the feed composition). Figure 7 presents results of the NO conversion (Fig. 7a) and N_2 selectivity (Fig. 7b) obtained in the 100–400°C range. For both catalysts the NO conversion increases significantly in the 100–200°C range and a smaller increase is observed in the 250–400°C range (Fig. 7a). $Pt/La_{0.7}Sr_{0.2}Ce_{0.1}FeO_3$ is found to exhibit significantly higher NO conversion values than Pt/SiO_2 in the 160–400°C range. A similar behavior is also obtained for the N_2 selectivity of the NO/H_2 reaction (Fig. 7b). It is also noted that the temperature profile of X_{NO} for the NO/H_2 reaction in the 100–400°C range is completely different than that obtained for the $NO/H_2/O_2$ reaction (Fig. 1a). At 100°C, a TOF_{N_2} value of 1.38×10^{-2} s^{-1} is calculated for the Pt/SiO_2, while a value of 2.02×10^{-2} s^{-1} is calculated for the $Pt/La_{0.7}Sr_{0.2}Ce_{0.1}FeO_3$ catalyst.

3.4. Kinetic Rates and Activation Energies of the NO/H₂/O₂, NO/O₂, and H₂/O₂ Reactions

In order to elucidate the catalytic activity behavior of the present supported Pt catalysts (Figs. 1, 2, and 6) kinetic

TABLE 4

Intrinsic Reaction Rates of NO/H_2/O_2, NO/O_2, and H_2/O_2 Reactions on Supported Pt Catalysts at $T = 140°C$

Catalyst	Reaction	Rate (μmol/g·s)	TOF (s^{-1})
0.1 wt% Pt/SiO_2	0.25% NO/1.0% H_2/5.0% O_2	1.41[a]	0.327
0.1 wt% Pt/$La_{0.7}Sr_{0.2}Ce_{0.1}FeO_3$		3.36[a]	0.747
0.1 wt% Pt/SiO_2	0.25% NO/5.0% O_2	0.009[a]	0.0021
0.1 wt% Pt/$La_{0.7}Sr_{0.2}Ce_{0.1}FeO_3$		0.045[a]	0.010
0.1 wt% Pt/SiO_2	1.0% H_2/5.0% O_2	71.3[b]	16.6
0.1 wt% Pt/$La_{0.7}Sr_{0.2}Ce_{0.1}FeO_3$		50.8[b]	11.3

[a] Micromoles of NO consumed per gram of catalyst per second.
[b] Micromoles of H_2 consumed per gram of catalyst per second.

studies were conducted. In particular, intrinsic rates of the NO/H_2/O_2, NO/O_2, and H_2/O_2 reactions at 140°C and the apparent activation energy of the NO/H_2/O_2 reaction for both catalyst formulations were estimated. The rate results obtained are given in Table 4 in terms of micromoles per gram of catalyst per second and TOF (per second) along with the feed composition used for each reaction. In the case of NO/O_2 reaction, only NO_2 was observed, with a rate value two orders of magnitude smaller than that observed for the desired NO/H_2/O_2 reaction. On the other hand, in the case of H_2 combustion the observed rate was 50 times higher than that of the NO/H_2/O_2 reaction in the case of Pt/SiO_2 and 15 times higher in the case of Pt/$La_{0.7}Sr_{0.2}Ce_{0.1}FeO_3$ catalyst. It is noted that no hydrogen combustion activity was observed for the supports alone at the same reaction conditions.

Figure 8 shows Arrhenius plots of $Ln(TOF_{N2})$ vs $1/T$ for the estimation of the apparent activation energy of the NO/H_2/O_2 reaction. Measurements were taken in the 70–120°C range with a feed consisting of 0.25% NO/1% H_2/5% O_2/He. Apparent activation energy values of 20.9 and 25.8 kcal/mol were calculated for the Pt/$La_{0.7}Sr_{0.2}Ce_{0.1}FeO_3$ and Pt/SiO_2 catalysts, respectively.

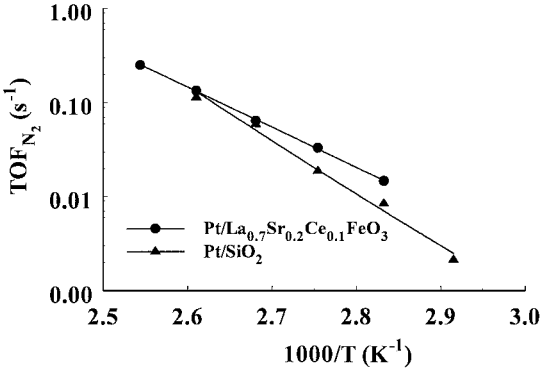

FIG. 8. Arrhenius plots of the rate (TOF, s^{-1}) of N_2 formation of the NO/H_2/O_2 lean de-NO_x reaction on the 0.1 wt% Pt/$La_{0.7}Sr_{0.2}Ce_{0.1}FeO_3$ (●) and 0.1 wt% Pt/SiO_2 (▲) catalysts. Feed composition: H_2 = 1.0%, NO = 0.25%, O_2 = 5%, He as balance gas.

3.5. *Surface Reactivity Studies by Transient Methods*

3.5.1. NO TPDs. Figure 9 shows the temperature-programmed desorption (TPD) response curves of NO,

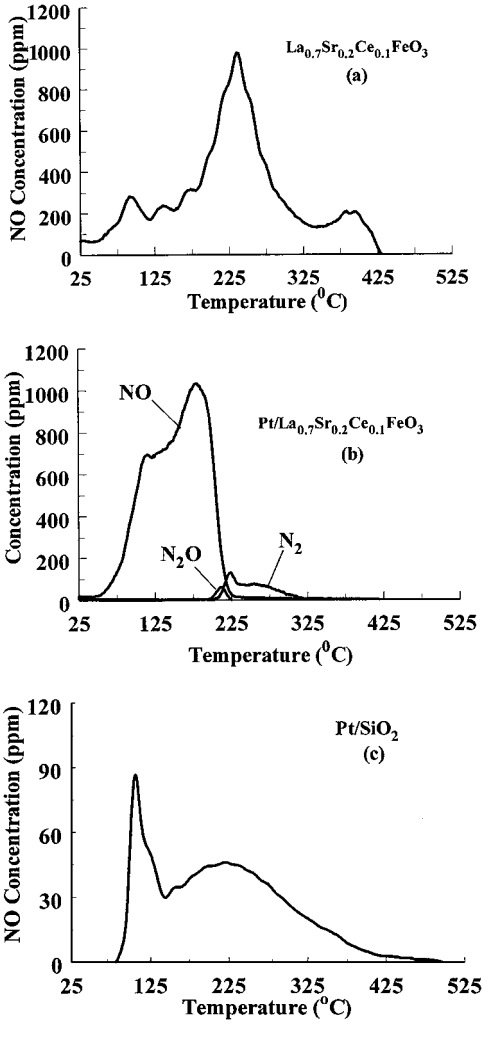

FIG. 9. Temperature-programmed desorption (TPD) profiles of NO, N_2, and N_2O in He flow according to Experiment A (Table 2) on (a) $La_{0.7}Sr_{0.2}Ce_{0.1}FeO_3$ ($W = 0.2$ g), (b) 0.1 wt% Pt/$La_{0.7}Sr_{0.2}Ce_{0.1}FeO_3$ ($W = 0.15$ g), and (c) 0.1 wt% Pt/SiO_2 ($W = 0.15$ g) catalysts. $\beta = 30°C/min$; $Q_{He} = 30$ cm^3/min.

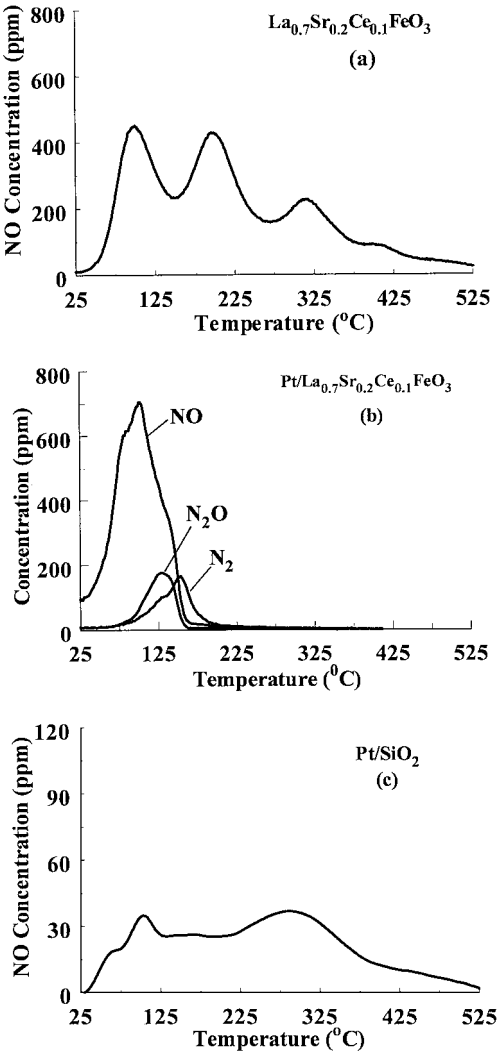

FIG. 10. Transient response curves of NO, N_2, and N_2O obtained during TPSR in He flow following reaction in $NO/H_2/O_2$ on the (a) $La_{0.7}Sr_{0.2}Ce_{0.1}FeO_3$, (b) 0.1 wt% $Pt/La_{0.7}Sr_{0.2}Ce_{0.1}FeO_3$, and (c) 0.1 wt% Pt/SiO_2 catalysts according to the sequence of steps described in Experiment B (Table 2). $Q_{He} = 30\,cm^3/min$; $\beta = 30°C/min$.

N_2O, and N_2 for all the studied solids (Experiment A, Table 2). Before NO chemisorption took place, $La_{0.7}Sr_{0.2}Ce_{0.1}FeO_3$ and SiO_2 solids were pretreated with 20% O_2/He (30 cm^3/min) at 650°C for 2 h, while the supported Pt catalyst samples were pretreated at 400°C for 2 h followed by H_2 treatment at 300°C for 2 h.

In the case of $La_{0.7}Sr_{0.2}Ce_{0.1}FeO_3$ (Fig. 9a), one distinct NO desorption peak is obtained ($T_M = 230°C$) with smaller desorption peaks (not well resolved) at the rising part of it. A small NO desorption peak is also obtained at higher temperatures ($T_M = 390°C$). In the case of $Pt/La_{0.7}Sr_{0.2}Ce_{0.1}FeO_3$ (Fig. 9b), the transient response curves of NO, N_2O, and N_2 are observed. A broad NO peak is observed in the 25–225°C range with a shoulder at the rising part of it, while a small broad N_2 peak is obtained in the 200–325°C range. A very small N_2O peak is centered at 195°C.

In the case of SiO_2, neither NO nor any other N-containing species was observed to desorb from its surface. In the case of Pt/SiO_2 (Fig. 9c), a sharp NO peak is centered at about 110°C, while a second broad peak is centered at 225°C. It is found that Pt/SiO_2 adsorbs about eight times less NO than the $Pt/La_{0.7}Sr_{0.2}Ce_{0.1}FeO_3$ catalyst (see Table 5, Experiment A). In addition, all adsorbed NO desorbs practically at $T < 200°C$ in the case of $Pt/La_{0.7}Sr_{0.2}Ce_{0.1}FeO_3$, while only 40% of NO does in the case of Pt/SiO_2.

3.5.2. TPSR in He flow following $NO/H_2/O_2$ reaction. Figures 10a–10c present the transient response curves of NO, N_2O, and N_2 obtained over $La_{0.7}Sr_{0.2}Ce_{0.1}FeO_3$, $Pt/La_{0.7}Sr_{0.2}Ce_{0.1}FeO_3$, and Pt/SiO_2 catalysts, respectively, according to Experiment B described in Table 2. In the case of $La_{0.7}Sr_{0.2}Ce_{0.1}FeO_3$ solid, three NO desorption peaks are clearly observed. The first two peaks are of the same peak maximum intensity and are centered at 100 and 200°C, respectively. The third smaller peak appears at 315°C with a tail out to 550°C. In the case of $Pt/La_{0.7}Sr_{0.2}Ce_{0.1}FeO_3$ (Fig. 10b) three peaks are observed, corresponding to NO, N_2O, and N_2. The NO peak is centered at 90°C, while the sharper N_2O peak is centered at 120°C. The N_2 peak appears at 155°C with a shoulder at the rising part of it. As is seen, all peaks appear at temperatures lower than 200°C, as opposed to the case of $La_{0.7}Sr_{0.2}Ce_{0.1}FeO_3$, where only NO desorbs. Part of the latter species desorbs at much higher temperatures compared to the case of supported Pt catalyst.

In the case of Pt/SiO_2 (Fig. 10c) a small NO peak is centered at about 110°C with a shoulder at the rising part of it, while a second broad peak is centered at 270°C with a tail out to 550°C. Table 5 (Experiment B) reports the amounts of NO, N_2O, and N_2 measured by the He TPSR experiments

TABLE 5

Amount of Species Desorbed ($\mu mol/g_{cat}$) during Various Kinds of Temperature-Programmed Desorption (TPD) and Surface Reaction (TPSR) Experiments in Different Gas Atmospheres as a Function of Catalyst Composition

Catalyst sample	Expt (Table 2)	NO	N_2O	N_2	Total N-containing species
0.1% $Pt/La_{0.7}Sr_{0.2}Ce_{0.1}FeO_3$	A	11.3	0.1	1.3	14.1 ($\theta = 3.1$)
	B	7.3	1.8	1.9	14.7 ($\theta = 3.25$)
	C	9.6		2.6	14.8 ($\theta = 3.3$)
0.1% Pt/SiO_2	A	1.7			1.72 ($\theta = 0.38$)
	B	2.2			2.2 ($\theta = 0.48$)
	C	1.1		0.6	2.3 ($\theta = 0.5$)
$La_{0.7}Sr_{0.2}Ce_{0.1}FeO_3$	A	12.2			12.2
	B	10.2			10.2

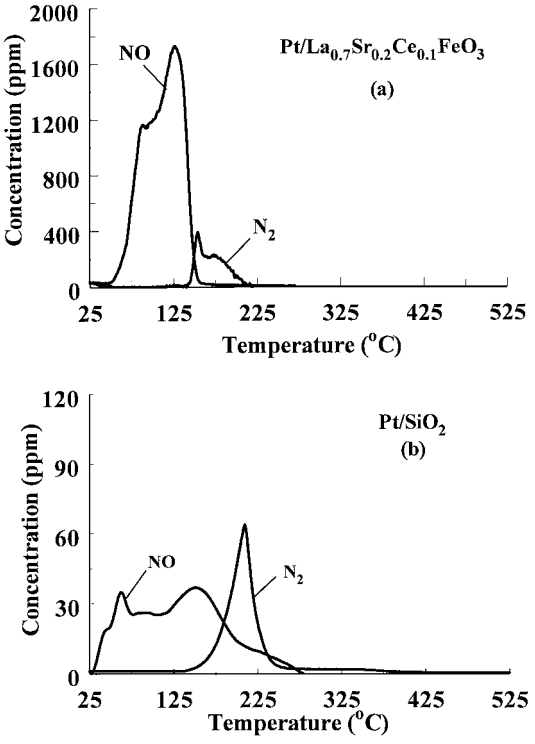

FIG. 11. Transient response curves of NO and N_2 gaseous species obtained during TPSR in 10% H_2/He flow following reaction in NO/H_2/O_2 on the (a) 0.1 wt% Pt/$La_{0.7}Sr_{0.2}Ce_{0.1}FeO_3$ and (b) 0.1 wt% Pt/SiO_2 catalysts according to the sequence of steps described in Experiment C (Table 2). $Q = 30$ cm^3/min; $\beta = 30$°C/min.

presented in Figs. 10a–10c. Also, the total amount of N-containing species and the individual surface coverage (θ) of each species (evaluated on the basis of Pt dispersion) are given in Table 5, last column.

3.5.3. TPSR in H_2/He flow following NO/H_2/O_2 reaction. Figures 11 and 12 describe the TPSR response curves of NO, N_2, and N_2O obtained in H_2/He flow according to Experiment C described in Table 2 on the Pt/$La_{0.7}Sr_{0.2}Ce_{0.1}FeO_3$ and Pt/SiO_2 catalysts (Fig. 11) and on the Pt/CeO_2 and Pt/Fe_2O_3 catalysts (Fig. 12). In the case of Pt/$La_{0.7}Sr_{0.2}Ce_{0.1}FeO_3$ (Fig. 11a), response curves corresponding to NO and N_2 are obtained. A desorption peak of NO centered at 125°C with a shoulder at the rising part of it is observed. A smaller N_2 peak centered at 155°C with a shoulder at the falling part of it is also observed. In the case of Pt/SiO_2 (Fig. 11b), a desorption peak of NO is obtained at 70°C and a broader one at 150°C. In addition, a sharp N_2 peak is observed at 215°C. By comparing the TPSR results of Figs. 10 and 11 two main differences must be pointed out. First, the TPSR response curves obtained in H_2/He flow are located at much lower temperatures than the corresponding ones in He flow. Second, the amounts of N_2 obtained on both catalysts in the case of TPSR are larger in H_2/He than He flow. The amounts of desorbed species are reported in Table 5 (Experiment C). In the case of Pt/CeO_2 and Pt/Fe_2O_3 catalysts (Fig. 12), only small amounts of N_2O are obtained, 0.65 and 0.7 μmol/g, respectively, in the 25–225°C range.

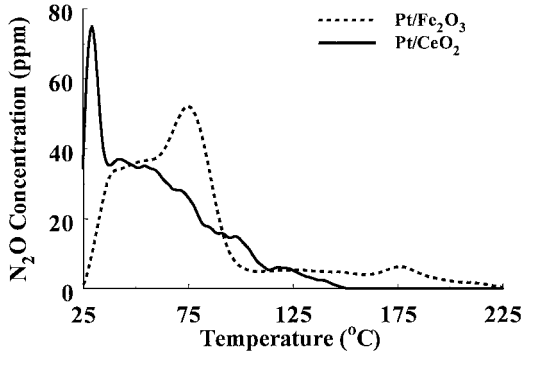

FIG. 12. Transient response curves of N_2O obtained during TPSR in 10% H_2/He flow following reaction in NO/H_2/O_2 on the 0.1 wt% Pt/CeO_2 and 0.1 wt% Pt/Fe_2O_3 catalysts according to the sequence of steps described in Experiment C (Table 2). $Q = 30$ cm^3/min; $\beta = 30$°C/min.

4. DISCUSSION

In a previous publication (24) we reported results on the catalytic performance of a 0.1 wt% Pt/La–Ce–Mn–O system toward the NO/H_2/O_2 reaction. The latter catalyst composition was found to exhibit a very high maximum specific integral reaction rate of N_2 formation at 140°C, with a value similar to the one obtained with the present 0.1 wt% Pt/La–Sr–Ce–Fe–O system at 160°C (see Table 6). However, the overall catalytic performance of the latter catalyst composition developed and presented here possesses significant advantages over that exhibited by the Pt/La–Ce–Mn–O solid composition. The main advantage with practical applications could be said to be the very high N_2 product yield measured at 140°C after a 20-h reaction on stream and in the presence of 5% H_2O in the feed. A value of 93% is obtained compared to the value of 78% obtained with the Pt/La–Ce–Mn–O catalytic system (Fig. 5 in Ref. (24)). This difference must be considered a significant improvement in catalyst development for an environmental catalytic reaction of such practical importance. Another advantage of the present Pt/La–Sr–Ce–Fe–O system compared to the Pt/La–Ce–Mn–O one (24) is the large improvement made in the operating temperature window (ΔT) in the 100–250°C low-temperature range. Defining ΔT as the temperature range within which the integral rate of N_2 formation appears to be greater than 1/2 of the maximum rate observed, values of about 110 and 60°C for the Pt/La–Sr–Ce–Fe–O and Pt/La–Ce–Mn–O catalysts, respectively, are obtained. In addition, for the same 100–250°C range the mean integral conversion of NO appears to be 72.6 and 55.7% for Pt/La–Sr–Ce–Fe–O and Pt/La–Ce–Mn–O, respectively. It is also

TABLE 6

Catalytic Activity of Various Supported Pt Catalysts for the $NO/H_2/O_2$ Reaction in the Low-Temperature Range of 90–200°C

Catalyst	Reaction conditions					R_{N_2}	ΔT_1	ΔT_2	X_{NO}	S_{N_2}	$TOF_{N_2} \times 10^2$	Ref.
	NO (%)	H_2 (%)	O_2 (%)	GHSV (h^{-1})	T_{max} (°C)	(μmol/s · g_m)	(°C)[a]	(°C)[b]	(%)	(%)	(s^{-1})[c]	
1% Pt/SiO_2	0.05	0.2	6	240,000	90	7.6	25	60	75	30	1.63[g]	18
1% Pt/Al_2O_3	0.05	0.2	6	240,000	140	10.1	40	90	50	60	0.87[h]	18
1% Pt/TiO_2	0.1	0.3	5.0[d]	40,000	100	2.2	50	100	50	21	0.17[g]	19
1% Pt/Al_2O_3	0.1	0.3	5.0[d]	40,000	100	1.4	65	120	62.2	11	0.22[g]	19
1% Pt–Mo–Co/Al_2O_3	0.3	0.8	8.0	6,500	150	12.1	30	70	55	50	0.31[h]	17
0.1% Pt/Al_2O_3	0.25	1.0	5.0[e]	80,000	125	285.8	45	100	66	60	26.5[g]/8.2[i]	24
0.1% $Pt/La_{0.5}Ce_{0.5}MnO_3$	0.25	1.0	5.0[e]	80,000	140	396.9	60	300[f]	88	79	49.0[g]/9.7[i]	24
0.1% Pt/SiO_2	0.25	1.0	5.0[e]	80,000	120	240.1	60	80	80	65	11.3[i]	This work
0.1% Pt/CeO_2	0.25	1.0	5.0	80,000	150	200.0	300	300	83	42		This work
0.1% $Pt/La_{0.7}Sr_{0.2}Ce_{0.1}FeO_3$	0.25	1.0	5.0[e]	80,000	160	443.5	100	300	90	92	13.4[i]	This work

[a] ΔT_1, Temperature range where $X_{NO} > X_{NO_{max}}/2$.
[b] ΔT_2, Temperature range where $X_{NO} > X_{NO_{max}}/10$.
[c] Using the reported $NO/H_2/O_2$ feed stream and for $X_{NO} < 15\%$.
[d] 10% H_2O is also present in the feed stream.
[e] 5% H_2O is also present in the feed stream.
[f] Except at $T = 250$°C.
[g] Evaluated at 140°C.
[h] Evaluated at 130°C.
[i] Evaluated at 110°C.

important to note that the Pt/La–Sr–Ce–Fe–O solid results in a significant increase in N_2 selectivity and yield for the $NO/H_2/O_2$ reaction when 5% H_2O is added in the feed. This result was not observed on the Pt/La–Ce–Mn–O solid previously investigated in this laboratory (24). The transient experiments presented in Figs. 9–12, which are similar to the ones performed on Pt/La–Ce–Mn–O catalyst, and the catalytic results obtained with Pt/CeO_2 and Pt/Fe_2O_3 solids (Fig. 6) aim to shed some light on our understanding about the intrinsic reasons that make the catalytic behavior observed on Pt/La–Sr–Ce–Fe–O much better than that of Pt/La–Ce–Mn–O. The significance of these results is discussed below.

4.1. Intrinsic Reasons of the Catalytic Performance of Pt/La–Sr–Ce–Fe–O Solid

For the present catalytic reaction, Table 6 reports maximum integral rates of N_2 production per gram of Pt metal (R_{N_2}) and also turnover frequencies, TOF(s^{-1}), for the best catalyst formulations reported. The comparison between the Pt/La–Sr–Ce–Fe–O and Pt/SiO_2 catalysts presently investigated is rather straightforward. The maximum specific integral rate of N_2 formation for the $NO/H_2/O_2/H_2O$ reaction when Pt is supported on $La_{0.7}Sr_{0.2}Ce_{0.1}FeO_3$ is about 85% higher than when supported on SiO_2 solid. In addition, a N_2 selectivity value of 92% obtained on $Pt/La_{0.7}Sr_{0.2}Ce_{0.1}FeO_3$, to our knowledge, is the highest value ever reported for the reaction at hand in the 100–200°C low-temperature range. According to the results in Table 6 and what has been discussed in the previous paragraph, the present $Pt/La_{0.7}Sr_{0.2}Ce_{0.1}FeO_3$ catalyst appears to be superior in all respects of its performance to all other supported Pt catalysts listed.

The fact that the present Pt/La–Sr–Ce–Fe–O, Pt/SiO_2, and Pt/CeO_2 catalysts exhibit similar dispersions (84–92%), a purely support effect must be invoked to explain the differences in their catalytic performance. It is suggested that the main reasons that $Pt/La_{0.7}Sr_{0.2}Ce_{0.1}FeO_3$ catalyst exhibits remarkable N_2 selectivity and activity values compared to Pt/SiO_2, Pt/CeO_2, and Pt/Al_2O_3 (24) catalysts is the ability of $La_{0.7}Sr_{0.2}Ce_{0.1}FeO_3$ support to

(a) regulate the hydrogen coverage on Pt toward an increase in reaction rate and N_2 selectivity;

(b) facilitate the storage of adsorbed NO_x species (e.g., NO_2^- and NO_3^-), the latter being formed by various routes of oxidation of NO, where the reduction of NO_x by H_2 to form N_2 gas on Pt might be considered to proceed at higher rates than the reduction of molecular NO;

(c) promote the formation of adsorbed NO species on oxygen vacant sites, the reduction of which proceeds at a higher rate than that of chemisorbed NO on Pt metal; and

(d) promote an electron transfer between the Pt metal and the support in a direction that favors the formation of N_2 over N_2O.

The above-mentioned ideas are elaborated in what follows.

A recent kinetic study of the $NO/H_2/O_2$ reaction on Pt–Mo–Co/α-Al_2O_3 catalyst (17) revealed that for O_2 feed concentrations below 2 mol% both the rate of NO conversion and the N_2 selectivity increase significantly with increasing O_2 feed concentration. The authors have suggested that the oxygen-promoting effect is attributed to the lowering

of the surface coverage of adsorbed hydrogen by reaction with oxygen to form H_2O, permitting therefore the pairing of two adjacent adsorbed N atoms to form N_2 gas. In the present work, the following results probe for the significance of θ_H to control catalyst activity and N_2 selectivity for the reaction at hand. First, higher N_2 selectivity values are obtained in the 100–160°C range in the presence rather than the absence of O_2 in the feed stream (see Figs. 1a and 7b). Second, the rate of combustion of H_2 to form water was found to be about 40% lower on Pt/$La_{0.7}Sr_{0.2}Ce_{0.1}FeO_3$ compared to Pt/SiO_2 (Table 4), where the latter catalyst exhibits lower N_2 selectivity values than the former one. Third, while Pt/CeO_2 presents a N_2 selectivity value of 45% at 150°C (NO/H_2/O_2 reaction conditions), in the presence of 10% H_2/He gas mixture (during the H_2 TPSR; Fig. 12) the NO_x species formed under NO/H_2/O_2 reaction conditions were reduced exclusively to N_2O gas.

Based on the above-mentioned ideas, it is reasonable to suggest that θ_H must be viewed as an important kinetic parameter of which the adjustment is important for N_2 selectivity maximization. One of the processes that would influence θ_H is that of the reaction of adsorbed hydrogen atoms on Pt with reactive oxygen species at the interface between the Pt particles and support. The $La_{0.7}Sr_{0.2}Ce_{0.1}FeO_3$ solid consists of the oxidic phases of CeO_2 and Fe_2O_3, and also the $LaFeO_3$ and $SrFeO_{3-x}$ perovskite-type phases, where Pt was highly dispersed within their pore structure. The CeO_2, the $LaFeO_3$, and particularly the $SrFeO_{3-x}$ phases (27) contain inherently a significant concentration of oxygen vacancies according to O_2 chemisorption experiments performed on the $La_{0.7}Sr_{0.2}Ce_{0.1}FeO_3$ solid (36.5 μatoms O/g_{cat}). This value is about eight times larger than the amount of exposed Pt atoms in the present Pt/$La_{0.7}Sr_{0.2}Ce_{0.1}FeO_3$ catalyst. The low N_2 selectivity values observed on Pt/CeO_2 and Pt/Fe_2O_3 catalysts (Fig. 6) may suggest that these oxidic phases cannot be responsible for the high N_2 selectivity values obtained by the Pt/La–Sr–Ce–Fe–O system, which the former catalysts belong to. It appears that the $LaFeO_3$ and $SrFeO_{3-x}$ support phase compositions are responsible for the high N_2 selectivities obtained with the Pt/La–Sr–Ce–Fe–O system. It could be argued that the $SrFeO_{3-x}$ phase, with a much higher concentration of ordered oxygen vacancies in its crystal structure per gram of solid compared to that of $LaFeO_3$ (27), provides atomic oxygen with appropriate mobility that could regulate θ_H in such a direction as to obtain optimum activity and N_2 selectivity.

It has been recently suggested (21) that on the 1 wt% Pt/TiO_2–ZrO_2 catalyst various kinds of nitrate species are responsible for determining the N_2 selectivity value of the NO/H_2/O_2 reaction. The reactivity of these species toward H_2 depends on their formation route. On the reduced Pt surface, nitrates should be formed from NO and O_2 chemisorbed onto Pt, while on the oxidized Pt surface nitrates may be formed from gaseous NO and oxygen chemisorbed onto Pt. The authors concluded that H_2/O_2 combustion is suppressed at low temperatures ($T < 150$°C) due to the fact that most of the Pt surface is covered by nitrate species. A recent work (28) concludes that Pt serves to oxidize not only NO to NO_2 but also NO_2 to NO_3^- on the Pt surface.

The NO TPDs shown in Figs. 9 and 10 strongly support the view of the existence of various kinds of NO_x species formed either on NO chemisorption at room temperature or after NO/H_2/O_2 reaction at 140°C. These adsorbed species are considered to be of the molecular type on Pt, and of nitrate and nitrite structure on the support and Pt metal (28–32). Important information revealed from the NO TPDs of Figs. 9 and 10 is that quantities of NO stored on Pt/La–Sr–Ce–Fe–O are about seven times larger than that stored on Pt/SiO_2 catalyst. In addition, significant amounts of NO_x species are stored on the La–Sr–Ce–Fe–O support itself (see Table 5). The kinetics of decomposition of these stored NO_x species in He flow or of their reduction in hydrogen flow toward N_2 or N_2O formation as a function of temperature strongly depends on the catalyst composition (Figs. 11 and 12).

The fact that the amount (micromoles per gram) of N_2 produced during the H_2 TPSR experiment is much higher on Pt/La–Sr–Ce–Fe–O than on Pt/SiO_2 (Table 5), Pt/CeO_2 (Fig. 12), and Pt/Fe_2O_3 catalysts (Fig. 12) could explain the higher N_2 specific activities observed on the Pt/La–Sr–Ce–Fe–O catalyst compared with those on the other ones. In addition, for the same H_2 TPSR experiment the Pt/La–Sr–Ce–Fe–O exhibits six times higher amounts per gram of solid of NO_x reduced to N_2 than does the Pt/La–Ce–Mn–O catalyst (24). This important result provides a good explaination for the higher N_2 yield exhibited by the former compared with the latter catalyst. It is noted that both La–Sr–Ce–Fe–O and La–Ce–Mn–O carriers have practically the same BET area.

Anionic vacant sites (F-type defects) mostly present in $SrFeO_{3-x}$, $LaFeO_3$, and CeO_2, but not SiO_2, phases are offered for O_2 chemisorption (16, 27, 33, 34). The presence of F-type defects in the $La_{0.7}Sr_{0.2}Ce_{0.1}FeO_3$ support, particularly in the $SrFeO_{3-x}$ phase, as previously discussed, and the fact that NO can be adsorbed onto these sites (35) make possible the likelihood of the formation of adsorbed NO_x species at the metal–support interface. In this chemisorbed state the N atom is bonded to the Pt metal and one oxygen atom is placed in the oxygen vacancy adjacent to a metal cation. This possibility is not offered in the case of Pt/SiO_2 and Pt/Al_2O_3. The strength of the N–O bond might be weaker than the corresponding one in the case of Pt–N=O adsorbed species. *In situ* FTIR studies may provide the means to probe in a direct manner the presence of the above-mentioned adsorbed NO_x structures. This kind of investigation will be attempted and results will soon be reported. The fact that Pt/CeO_2 presents a remarkable activity toward NO conversion but low N_2 selectivity compared to that of the Pt/La–Sr–Ce–Fe–O system may suggest

that the NO_x species associated with oxygen vacant sites, even though they may possess lower N–O bond strengths, are not selectively reduced to N_2 gas, the latter because of the less favored chemical conditions encountered on the Pt/CeO_2 surface compared to the Pt/La–Sr–Ce–Fe–O one. Therefore, it is suggested that the $LaFeO_3$ and particularly the $SrFeO_{3-x}$ crystal phase present in the Pt/La–Sr–Ce–Fe–O system promote the storage of higher amounts than the Pt/SiO_2 catalyst of more reactive NO_x species toward their reduction by hydrogen to form N_2 gas. It is important to note here that the low value of the steady state rate of NO_2 formation during NO/O_2 reaction (Table 4) does not imply the absence of a large reservoir of adsorbed NO_x ($x = 2, 3$) on the metal and/or support.

It has been reported (36, 37) that $LaFeO_3$ and $La_{1-x}Sr_xFeO_{3-\delta}$ perovskite-type oxides are considered p-type semiconductors. To our knowledge, no information is available on the values of work function of these materials. Depending on their Fermi level, a higher or lower Fermi energy value than that exhibited by Pt (∼5.7 eV) would result in an electron transfer from the Pt metal to the $LaFeO_3$ and $La_{1-x}Sr_xFeO_{3-\delta}$ support phases or vice versa, according to the metal–semiconductor contact theory (38–40). The result then would be the electron depletion or enrichment of the Pt d-band. This important electronic effect would affect the bonding interaction of significant active intermediate species that eventually lead to N_2 and N_2O, thus controlling the reaction rate and N_2 selectivity. However, the issue as to which reaction elementary steps have been favorably influenced by such an electron transfer is the most difficult one to address. Given the high dispersion of the Pt clusters in the present catalytic system, and the semiconductor-type nature of some of the support phases, it is suggested that Pt–support electronic interactions cannot be excluded to justify the remarkable performance of $Pt/La_{0.7}Sr_{0.2}Ce_{0.1}FeO_3$ compared to that of Pt/SiO_2 and Pt/Al_2O_3 (24) catalysts (see Table 6).

The present $La_{1-x-y}Sr_xCe_yFeO_3$ series of solids were also investigated for the reduction of NO by CO in the 200–500°C range (25). It was found that the $La_{0.7}Sr_{0.2}Ce_{0.1}FeO_3$ solid had the highest TOF_{NO} value at 300°C, while the solid composition with increasing concentration in $SrFeO_{3-x}$ and CeO_2 phases resulted in an increasing catalytic activity. In explaining this behavior, it was pointed out (25) that the $SrFeO_{3-x}$ phase contains the iron in two oxidation states, +3 and +5, according to Mössbauer results. If such a crystal $Sr(Fe^{3+}, Fe^{5+})O_{3-x}$ has surface sites for adsorption and catalysis and is in contact with CeO_2 crystals via another part of its surface, a solid electromotive cell with redox cycles can be visualized to be operative. A redox interaction for the CuO_x/CeO_2 system has also been proposed toward CO oxidation (41). In addition, Bentrup *et al.* (42) recently studied NO_x adsorption on MnO_2/NaY catalyst by *in situ* EPR experiments. They concluded that the reducible manganese species that support the oxidation of NO to nitrite and then to nitrate species are important. The aforementioned redox mechanism promoted by the synergy of $SrFeO_{3-x}$ and CeO_2 phases might be another way of explaining the catalytic activity and N_2 selectivity of $Pt/La_{0.7}Sr_{0.2}Ce_{0.1}FeO_3$ (Figs. 1a and 3). In fact, while Pt/CeO_2 alone has remarkable catalytic activity behavior (Fig. 6a), the N_2 selectivity exhibited is much lower than that obtained on the Pt/La–Sr–Ce–Fe–O system. This result supports the above-mentioned view about the synergy of $SrFeO_{3-x}$ and CeO_2 phases.

4.2. Catalyst Activity Behavior with Temperature, Time on Stream, and Water Content in the Feed

The maximum in the activity-versus-temperature profile observed at 160°C (Figs. 1a and 2a) is clearly due to the significant rate of H_2 combustion to H_2O on the Pt surface according to the results of Fig. 1b and the kinetic rates reported in Table 4. Ueda *et al.* (19) also measured a rate of H_2 combustion at 300°C on the 1 wt% Pt/Al_2O_3 catalyst 30 times larger than that obtained for the NO/H_2 reaction. According to the catalytic results of the present $Pt/La_{0.7}Sr_{0.2}Ce_{0.1}FeO_3$, Pt/SiO_2, and $La_{0.7}Sr_{0.2}Ce_{0.1}FeO_3$ solids, the activity-versus-temperature profile in the 100–400°C range is due to the bifunctional operation of the catalyst. The Pt metal operates in the 100–200°C range, while the $La_{0.7}Sr_{0.2}Ce_{0.1}FeO_3$ support operates in the 250–400°C range, where the activity of the latter is somehow influenced by the Pt metal. The remarkable activity-versus-temperature profile obtained with the Pt/CeO_2 catalyst in the 100–400°C range (Fig. 6a), largely different than that obtained with the Pt/La–Sr–Ce–Fe–O system (Fig. 1a), strongly suggests that a low weight percent content of CeO_2 is present in the $La_{0.7}Sr_{0.2}Ce_{0.1}FeO_3$ support (Table 3). Along with what was discussed in the previous section, this result reveals the importance of the other two support phases present, e.g., $SrFeO_{3-x}$ and $LaFeO_3$, in determining both activity and N_2 selectivity for the reaction at hand.

The remarkable stability-test results observed on $Pt/La_{0.7}Sr_{0.2}Ce_{0.1}FeO_3$ (Fig. 5), where a continuous increase in N_2 yield is observed during the 5–20 h on stream, require some explanation. It is clear that there must exist a time-dependent parameter that influences the present catalytic phenomenon. To shed some light on this aspect, the effect of water on the rate of reduction of NO was studied and the results obtained are as follows.

The steady state rate of water decomposition in the 100–400°C range was measured on Pt/SiO_2, $Pt/La_{0.7}Sr_{0.2}Ce_{0.1}FeO_3$, $La_{0.7}Sr_{0.2}Ce_{0.1}FeO_3$, CeO_2, and Fe_2O_3 solids after using a 5% H_2O/He gas mixture and measuring the production of hydrogen by *online* mass spectrometry. On the latter three solids no measurable reaction rate was observed. However, on Pt/SiO_2 a rate of 3.4×10^{-3} and

0.65×10^{-3} (μmol/g · s) at 300 and 150°C, respectively, was estimated, while on Pt/$La_{0.7}Sr_{0.2}Ce_{0.1}FeO_3$ the corresponding rates were found to be 4.1×10^{-3} and 0.8×10^{-3} (μmol/g · s). TPD of water (after adsorption at 30°C from a 5% H_2O/He mixture) revealed that Pt/SiO_2 catalyst adsorbs four times less water (per gram of solid) than the Pt/$La_{0.7}Sr_{0.2}Ce_{0.1}FeO_3$ catalyst. In addition, water desorbs from the latter catalyst at higher temperatures than from the former catalyst.

Based on the above-mentioned results and the N_2 reaction rates reported in Table 6, it is difficult to support the view that a slow process of water spillover from the $La_{0.7}Sr_{0.2}Ce_{0.1}FeO_3$ support onto the Pt metal followed by water dissociation to atomic hydrogen could explain the results in Fig. 5. It is noted that even though the conversion of H_2 at the experimental conditions reported in Fig. 5 is more than 85%, the rate of H_2 production by water decomposition is about two orders of magnitude smaller than the rate of NO/H_2/O_2 reaction. However, a mechanism involving an activated water dissociation step onto the La–Sr–Ce–Fe–O support surface that could provide hydrogen that by a back-spillover process would be adsorbed onto the Pt surface may not be excluded. If such a process is operated on the present Pt/La–Sr–Ce–Fe–O system, it should imply that an increase in θ_H must favor the N_2 yield. However, the H_2 TPSR results in Fig. 12 and the N_2 selectivity values reported in Fig. 1a do not support such a mechanism. On the other hand, the role that θ_H plays on the N_2 yield over the Pt/$SrFeO_{3-x}$ and Pt/$LaFeO_3$ catalytic systems remains unknown.

Hodjati *et al.* (43) and Eguchi *et al.* (44) have reported results on the beneficial effect of H_2O on the adsorptive capacity of some perovskites ABO_3 (A = Ca, Sr, Ba and B = Sn, Zr, Ti) and Mn–Zr–O mixed oxides toward NO and NO_2 under lean-burn conditions. The authors have suggested that adsorbed water stabilizes adsorbed NO_3^- species through hydration, with the latter being formed via NO and NO_2 adsorption. Along these lines, the slow accumulation of NO_3^- species on the $La_{0.7}Sr_{0.2}Ce_{0.1}FeO_3$ support and at the interface between Pt metal and the support might be considered one of the reasons for the increasing activity of N_2 formation with time on stream on the Pt/$La_{0.7}Sr_{0.2}Ce_{0.1}FeO_3$ catalyst (Fig. 5).

4.3. Transient Studies

4.3.1. NO TPDs. In the case of Pt/$La_{0.7}Sr_{0.2}Ce_{0.1}FeO_3$ and its support alone, the adsorption amount of NO on Pt (based on the results obtained for the Pt/SiO_2 catalyst) and $La_{0.7}Sr_{0.2}Ce_{0.1}FeO_3$ support obeys the additive rule when compared to the adsorption amount obtained on the Pt/$La_{0.7}Sr_{0.2}Ce_{0.1}FeO_3$. However, the NO TPD spectra (shape and position) obtained on $La_{0.7}Sr_{0.2}Ce_{0.1}FeO_3$ and Pt/$La_{0.7}Sr_{0.2}Ce_{0.1}FeO_3$ solids are quite different. These results clearly indicate that small Pt clusters deposited onto the $La_{0.7}Sr_{0.2}Ce_{0.1}FeO_3$ support have considerably altered the binding energy of certain type(s) of NO_x adsorbed species on the support and their reactivity characteristics via short-range electronic interactions (Section 4.1). The various NO TPD peaks observed in Fig. 9a can be justified based on the fact that chemisorption of NO on metal oxides proceeds with the participation of metal cations, oxygen anions, and oxygen vacant sites, as previously discussed.

The N_2 and N_2O response curves seen in the TPDs on Pt/$La_{0.7}Sr_{0.2}Ce_{0.1}FeO_3$, and not seen on the $La_{0.7}Sr_{0.2}Ce_{0.1}FeO_3$ and Pt/SiO_2 solids, strongly suggest that Pt/$La_{0.7}Sr_{0.2}Ce_{0.1}FeO_3$ facilitates the breaking of the N–O bond even in the absence of hydrogen. The following widely accepted elementary reaction steps describe the formation of N_2 and N_2O on the Pt surface:

$$\text{NO(g)} + \text{s} \leftrightarrow \text{NO-s}, \quad [9]$$

$$\text{NO-s} + \text{s} \rightarrow \text{N-s} + \text{O-s}, \quad [10]$$

$$\text{NO-s} + \text{N-s} \rightarrow \text{N}_2\text{O(g)} + 2\text{s}, \quad [11]$$

$$\text{N-s} + \text{N-s} \rightarrow \text{N}_2\text{(g)} + 2\text{s}. \quad [12]$$

In the case of Pt/SiO_2, two adsorbed states of NO_x are clearly formed with the participation of Pt clusters (Fig. 9c); no adsorption of NO on SiO_2 support was observed. A NO TPD spectrum different in shape and position from that shown in Fig. 9c has been reported by Burch *et al.* (45) with the 5 wt% Pt/SiO_2 catalyst. In addition, two N_2 and N_2O desorption peaks were observed (45), a result opposite that obtained on the present 0.1 wt% Pt/SiO_2 catalyst. These results may indicate that adsorption and surface reaction processes of NO on the Pt/SiO_2 catalyst may be considered structure-sensitive ones. It is also interesting to note that the NO TPDs obtained on Pt/$La_{0.5}Ce_{0.5}MnO_3$ (24) have shown much less propensity for NO dissociation and lower binding energies for NO chemisorption. This might be one of the reasons for the better activity and N_2 selectivity values obtained on the Pt/$La_{0.7}Sr_{0.2}Ce_{0.1}FeO_3$ (Fig. 1a, Table 6) compared to that on the Pt/$La_{0.5}Ce_{0.5}MnO_3$ catalyst (24).

4.3.2. TPSR experiments in He and H_2 flow following NO/H_2/O_2 reaction. The differences in the spectra shown in Figs. 10b and 11a in the case of Pt/La–Sr–Ce–Fe–O concern the composition and amounts of gases evolved and therefore reflect the different kinetics of reactions that occurred under He or H_2 gas, respectively. The profile of desorbed NO in the H_2 TPSR (Fig. 11a) shifts significantly to lower temperatures compared to that obtained during He TPD (Fig. 9b) and TPSR (Fig. 10b) experiments. Based on these remarks and on the fact that two distinct NO_x adsorbed states are very likely to have been formed on this catalyst (Figs. 9b and 10b), the following discussion explains the results of Figs. 10b and 11a in a satisfactory manner.

A hydrogen-assisted effect on the lowering of bond strength of Pt–NO might be expected, as has been reported for a supported Rh catalyst (46). In the H_2 TPSR experiment, the coverage of adsorbed atomic hydrogen is expected to be higher than that found under $NO/H_2/O_2$ reaction conditions, while under NO/He adsorption conditions this species is not present. Therefore, the shift of NO response to lower temperatures in the H_2 TPSR (Fig. 11a) with respect to the ordinary NO TPD response (Fig. 9b) can be justified. We have previously suggested (24) that a hydrogen-assisted NO dissociation mechanism, first suggested by Hecker and Bell (8) for the Rh/SiO_2 catalyst, might be suitable to explain the H_2 TPSR results obtained on the Pt/La–Ce–Mn–O catalytic system.

It was reported (47) that the activation energy of the N–O bond dissociation step [9] is higher than that of the H-assisted N–O bond dissociation step

$$\text{NO-s} + \text{H-s} \rightarrow \text{N-s} + \text{OH-s}. \qquad [13]$$

Formation of H_2O proceeds via the elementary reaction step

$$\text{OH-s} + \text{H-s} \rightarrow \text{H}_2\text{O(g)} + 2\text{s}. \qquad [14]$$

A nitrogen-assisted NO reduction to N_2 and N_2O has been proposed (8, 47). It has been shown that formation of N_2 and N_2O via these mechanisms proceeds with a lower activation energy barrier than the recombination reaction step [12] of adsorbed atomic N to form N_2 gas. In the NO TPD of Fig. 9b little NO dissociation occurs (30% of adsorbed NO; Table 5). On the other hand, in the case of He TPSR some adsorbed atomic N might be present at the start of the experiment. This species could have been formed during $NO/H_2/O_2$ reaction. According to these results and those of Fig. 10b, the rate of nitrogen-assisted NO dissociation becomes significant even at low temperatures (100–150°C range) and competes favorably with the rate of NO desorption.

In the case of H_2 TPSR on Pt/SiO_2 (Fig. 11b), an amount of NO_x species four times lower than that corresponding to $Pt/La_{0.7}Sr_{0.2}Ce_{0.1}FeO_3$ was reduced to produce exclusively N_2 gas (Table 5). This reduction step of NO_x by hydrogen proceeds at lower temperatures for the latter than for the former catalyst. Therefore, the fact that the $Pt/La_{0.7}Sr_{0.2}Ce_{0.1}FeO_3$ catalyst was found to exhibit significantly higher N_2 selectivity values during the $NO/H_2/O_2$ reaction in the 100–200°C range compared to Pt/SiO_2 is in harmony with the H_2 TPSR results.

In the case of Pt/La–Sr–Ce–Fe–O catalyst, according to the H_2 TPSR results of Fig. 11a and Table 5, only one-third of the NO_x stored under $NO/H_2/O_2$ reaction conditions can be reduced to N_2 gas. The rest is desorbed as NO at $T < 130$°C. Thus, under the present reaction conditions it is likely that a large amount of NO_x species is *inactive* (spectator species). It is noted that in the case of Pt/La–Ce–Mn–O (24) during the H_2 TPSR experiment significant amounts of N_2O and smaller amounts of NH_3 were produced, a result totally different than the one presented in Fig. 11a. A similar behavior is obtained in the case of Pt/CeO_2 and Pt/Fe_2O_3 catalysts (Fig. 12). These results are in harmony with the fact that N_2 selectivity values on the Pt/La–Sr–Ce–Fe–O were higher than on the Pt/La–Ce–Mn–O catalyst (24). Again, this result shows the great effect of support in determining the surface catalytic chemistry of the $NO/H_2/O_2$ reaction on supported Pt catalysts at low temperatures.

5. CONCLUSIONS

The following conclusions can be derived from the results of the present work.

1. A 0.1 wt% Pt supported on $La_{0.7}Sr_{0.2}Ce_{0.1}FeO_3$ (a mixed oxide containing $LaFeO_3$, $SrFeO_{3-x}$, CeO_2, and Fe_2O_3 phases) has proven to give the highest maximum specific integral rate (μmol/g of Pt · s) of N_2 formation during $NO/H_2/O_2$ lean de-NO_x reaction in the 100–200°C low-temperature range ever reported in the open literature. In addition, a very high N_2 yield (93%) in the presence of 5% H_2O in the feed stream at 140°C and after 20 h on stream has been obtained. This result is by far better than that obtained on the 0.1 wt% Pt/SiO_2, 0.1 wt% Pt/Al_2O_3 (24), and 0.1 wt% Pt/La–Ce–Mn–O (24) catalysts tested at the same reaction conditions.

2. The remarkable catalytic behavior of 0.1 wt% $Pt/La_{0.7}Sr_{0.2}Ce_{0.1}FeO_3$ toward $NO/H_2/O_2$ reaction is suggested to be due to various direct and indirect influences of support composition, in particular of the $SrFeO_{3-x}$ phase, as indicated in Section 4.1.

3. At least two distinct adsorbed states of NO_x on the $Pt/La_{0.7}Sr_{0.2}Ce_{0.1}FeO_3$ and Pt/SiO_2 catalysts are observed to desorb in the 70–525°C range in He flow following adsorption of NO at room temperature or reaction in $NO/H_2/O_2$ gas mixture at 150°C.

4. Only a portion (about 35%) of the more strongly bound adsorbed state of NO_x was found to react with H_2 in the 125–250°C range to give N_2 gas following reaction in $NO/H_2/O_2$ at 140°C. The amount of the strongly bound adsorbed state of NO_x is found to be much higher in the case of Pt/La–Sr–Ce–Fe–O than Pt/SiO_2. In addition, it reacts with H_2 at higher temperatures in the case of Pt/SiO_2 than Pt/La–Sr–Ce–Fe–O catalyst and it is considered to represent the active pool of NO_x formed under reaction conditions.

5. The rate of oxidation of H_2 to form H_2O (using 1% H_2/5% O_2/He mixture) was found to be about 40% less on the $Pt/La_{0.7}Sr_{0.2}Ce_{0.1}FeO_3$ compared to the Pt/SiO_2 catalyst. This result may contribute to the higher N_2 selectivity values observed on the former catalyst, if the H-assisted NO dissociation step is an important reaction step.

ACKNOWLEDGMENTS

Financial support by the Research Committee of the University of Cyprus and the European Union (GROWTH-GRDI-2000-25043) is gratefully acknowledged. The experimental assistance of Christos Christofides and Niovi Michael (final-year-project students of this university) is also acknowledged.

REFERENCES

1. Fritz, A., and Pitchon, V., *Appl. Catal. B* **13**, 1 (1997).
2. Pârvulescu, V. I., Grange, P., and Delmon, B., *Catal. Today* **46**, 233 (1998).
3. Busca, G., Lietti, L., Ramis, G., and Berti, F., *Appl. Catal. B* **18**, 1 (1998).
4. Janssen, F. J., in "Handbook of Heterogeneous Catalysis" (G. Ertl, H. Knözinger, and J. Weitkamp, Eds.), p. 1633. VCH, Weinheim, 1997.
5. Rausenberger, B., Swiech, W., Schmid, A. K., Rastomjee, C. S., Emgel, W., and Bradshaw, A. M., *J. Chem. Soc., Faraday Trans.* **94**(7), 963 (1998).
6. Dumpelmann, R., Cant, N. W., and Trimm, D. L., in "3rd ICC and Automotive Polution Control, Brussels" (A. Frennet and J.-M. Bastin, Eds.), Vol. 2, p. 13, Université Libre De Bruxelles, Brussels, Belgium, 1994.
7. Tomishige, K., Asakura, K., and Iwasawa, Y., *J. Catal.* **157**, 472 (1995).
8. Hecker, W. C., and Bell, A. T., *J. Catal.* **92**, 247 (1985).
9. Hornung, A., Muhler, M., and Ertl, G., *Catal. Lett.* **53**, 77 (1998).
10. Kobylinski, T. P., and Taylor, B. W., *J. Catal.* **33**, 376 (1974).
11. Huang, S. J., Walters, A. B., and Vannice, M. A., *J. Catal.* **173**, 229 (1998).
12. Burch, R., and Scire, S., *Catal. Lett.* **27**, 177 (1994).
13. Salama, T. M., Ohnishi, R., Shido, T., and Ichikawa, M., *J. Catal.* **162**, 169 (1996).
14. Tanaka, T., Yokota, K., Doi, H., and Sugiura, M., *Chem. Lett.* 273 (1997).
15. Lindsteld, A., Strömberg, D., and Milh, M. A., *Appl. Catal.* **116**, 109 (1994).
16. Ferri, D., Forni, L., Dekkers, M. A. P., and Nieuwenhuys, B. E., *Appl. Catal. B* **16**, 339 (1998).
17. Frank, B., Emig, G., and Renken, A., *Appl. Catal. B* **19**, 45 (1998).
18. Burch, R., and Coleman, M. D., *Appl. Catal. B* **23**, 115 (1999).
19. Ueda, A., Nakao, T., Azuma, M., and Kobayashi, T., *Catal. Today* **45**, 135 (1998).
20. Yokota, K., Fukui, M., and Tanaka, T., *Appl. Surf. Sci.* **121/122**, 273 (1997).
21. Machida, M., Ikeda, S., Kurogi, D., and Kijima, T., *Appl. Catal. B* **35**, 107 (2001).
22. Burch, R., Millington, P. J., and Walker, A. P., *Appl. Catal. B* **4**, 160 (1994).
23. Fukui, M., Yokota, K., and Shokubai, K., *Catal. Catal.* **36**, 160 (1994).
24. Costa, C. N., Stathopoulos, V. N., Belessi, V. C., and Efstathiou, A. M., *J. Catal.* **197**, 350 (2001).
25. Belessi, V. C., Bakas, T. V., Costa, C. N., Efstathiou, A. M., and Pomonis, P. J., *Appl. Catal. B* **28**, 13 (2000).
26. Costa, C. N., Anastasiadou, T., and Efstathiou, A. M., *J. Catal.* **194**, 250 (2000).
27. Belessi, V. C., Costa, C. N., Bakas, T. V., Anastasiadou, T., Pomonis, P. J., and Efstathiou, A. M., *Catal. Today* **59**, 347 (2000).
28. Kikuyama, S., Matsukuma, I., Kikuchi, R., Sasaki, K., and Eguchi, K., *Appl. Catal. A* **5840**, 1 (2001).
29. Cunha, M. C. P. M., Weber, M., and Nart, F. C., *J. Electroanal. Chem.* **414**, 163 (1996).
30. Klingenberg, B., and Vannice, M. A., *Appl. Catal. B* **21**, 19 (1999), and references therein.
31. Xue, E., Seshan, K., and Ross, J. R. H., *Appl. Catal. B* **11**, 65 (1996).
32. Kladis, C., Bhargava, S. K., Foger, K., and Akolekar, D. B., *Catal. Today* **63**, 297 (2000).
33. Eguchi, K., Kondo, T., Hayashi, T., and Arai, H., *Appl. Catal. B* **16**, 69 (1998).
34. Tejuca, L. G., Fierro, J. L. G., and Tascon, J. M. D., *Adv. Catal.* **36**, 237 (1989).
35. Busca, G., and Lorenzelli, V., *J. Catal.* **72**, 303 (1981).
36. Mizusaki, J., Sasamoto, T., Cannon, W. R., and Bowen, H. K., *J. Am. Ceram. Soc.* **65**, 363 (1982).
37. Yi, G., Hayakawa, T., Andersen, A. G., Suzuki, K., Hamakawa, S., York, A. E., Shimizu, M., and Takehira, K., *Catal. Lett.* **38**, 189 (1996).
38. Schwab, G. M., *in* "Advances in Catalysis" (D. D. Eley, H. Pines, and P. B. Weisz, Eds.), Vol. 27, p. 1. Academic Press, New York, 1978.
39. Solymosi, F., *Catal. Rev.* **1**, 233 (1967).
40. Ioannides, T., and Verykios X. E., *J. Catal.* **161**, 560 (1996).
41. Shaw, E. A., Rayment, T., Walker, A. P., and Lambert, R. M., *Appl. Catal.* **67**, 151 (1990).
42. Bentrup, U., Bruckner, A., Richter, M., and Fricke, R., *Appl. Catal. B* **32**, 229 (2001).
43. Hodjati, S., Vaezzadeh, K., Petit, C., Pitchon, V., and Kiennemann, A., *Appl. Catal. B* **26**, 5 (2000).
44. Eguchi, K., Watabe, M., Ogata, S., and Arai, H., *J. Catal.* **158**, 420 (1996).
45. Burch, R., Shestov, A. A., and Sullivan, J. A., *J. Catal.* **186**, 353 (1999).
46. Solymosi, F., and Knozinger, H., *J. Chem. Soc. Faraday Trans.* **86**(2), 389 (1990).
47. Shustorovich, E., and Bell, A. T., *Surf. Sci.* **289**, 127 (1993).